Final Technical Report

Award #: G16AP00013

Title: **NEIC Implementation of Real-Time Earth Energy and Rupture Duration**

Authors:
Andrew V. Newman, Louisa Barama, Georgia Institute of Technology, 311 Ferst Drive, Atlanta, GA, 30332. 404-894-3976, 404-894-5638 (fax), anewman@gatech.edu

Period of performance: January 1, 2016 – Dec 31, 2016.

Abstract:
Over the past decade a number of globally distributed very large and great earthquakes has tested the upper limits of our current methodologies for rapidly assessing their size. Because rapid assessment of earthquake size is important for hazard mitigation from both strong shaking and potential tsunami generation, the U.S. Geological Survey's Earthquake Hazards Program has identified the issue and is calling for projects that "*supports efforts to improve the accuracy of algorithms and processes that provide information about earthquakes in near-real-time*" [*NEHRP*, 2015]. Because of this, we were funded in 2008 to extend the rapid radiated energy algorithms of *Newman and Okal* [1998] to assess the approximate rupture duration, radiated earthquake energy and energy magnitudes (M_E) of the largest observed earthquakes. Much like the well-established and nearly ubiquitous moment magnitude (M_W), M_E is directly related to a physical parameter (the amount of strong shaking radiated from an earthquake), and does not suffer from saturation, working rapidly and successfully for the largest and longest earthquakes recorded with modern seismic networks. These real-time codes have been operating in research-mode at Georgia Tech since January 2009, consistently providing near-real-time information through automated emails, text messages, and webpages with robust solutions normally appearing approximately 10 to 15 minutes after the initiation of earthquake rupture.
Building off of this research and code development that was originally supported by the NEHRP program, the project proposed here is aimed at directly implementing the now robust algorithms for real-time earthquake energy and rupture duration into the National Earthquake Information Center (NEIC). Specifically, with these funds:

1. We will fully implement a new and well-tested algorithm for rapid duration estimates (TACER [*Convers and Newman,* 2013]) that will provide for improved per-station energy and duration solutions, real-time error reporting, and generally more accurate results for most earthquakes.
2. Once implemented, we will recalculate energy and duration values for entire post-1997 catalog of earthquakes following the methods described in *Convers and Newman* [2011], as well as those reported by the NEIC (through to the time when hardware operating the then existing NEIC algorithms were taken out of operation in 2013).
3. From the newly developed catalog we will develop rich per-station statistics and will test algorithms and establish a new base line for which to evaluate future events.
4. Implement new codes at the NEIC for real-time warning information.
5. Perform six-month quality control and testing of new system with real-time activity one-unit magnitude lower than our reporting threshold (M_W 6.5) to ensure continued robust behavior.
6. Report on new system, and its response, at the 2016 Fall AGU meeting and in a new long-format peer-reviewed publication.

While providing improvements to existing codes, and developing new codes we continue to run be running automated detections using a stable version, with automatic online reporting at (http://geophysics.eas.gatech.edu/RTerg/). Because calculation speed is negligible, this methodology is expected to be highly useful for real-time early estimates of earthquake size.

Algorithm Development:
Through the duration of the award, we spent the bulk of our efforts working to improve observations of our development and implementation of the energy calculations using the improved methodology. Here, we developed new algorithms that tested and compared energy and duration results as obtained from the real-time network between 2009 and 2020 exploring the wealth of data collected from stations available to Georgia Tech machines through the USGS's development of the Continuous Waveform Buffer query tool (CWBQuery), after an initial detection of an event is identified using the Earthquake Information Distribution System (EIDS).

We run automatically and routinely for events with magnitude greater than 5.5, and currently run each event for 6 automatic iterations. Because data are gathered from teleseismic stations between 25° and 80° from a source, iterations are necessary to ensure data are collected from the growing number of stations as waveforms become available at sites further from an event. Generally, the iterations complete within 15-20 minutes from the initial nucleation of an earthquake, however we have been running slower recently due to software incompatibilities on an updated OS. This is temporary, and doesn't represent a true slow-down of code or long-term capabilities. Once results are determined for an individual iteration, they are automatically distributed via text messages, emails, and a webpage is generated (www.geophysics.eas.gatech.edu/anewman/research/rterg). We recalculated the energies and durations for the post-2009 dataset, as this is the window for which the algorithm is best adapted to.

We developed additional codes using the Obspy packages available for python, but ran into difficulties early on. These difficulties were a combination of changes between versions of the software, and our own technical capabilities with our new student worker that was primarily tasked with this development. As such, during the initial development of this code, we abandoned full implementation in Python (at least temporarily), and left the heavy lifting of the energy calculations to be performed with our updated FORTRAN codes.

Our algorithm now produces individual TACER results readily for all new events, and a rich dataset of durations as well as new energy estimates can be evaluated. For each event, TACER durations are determined at both broadband (0.5 and 70s periods) and high-frequency (0.5 and 2s periods) for each waveform that pass initial automatic inspection. Individual TACER results are reported as their azimuthal distribution about the event (Figure 1). For the event, the azimuthal distribution of TACER is shown along with the reporting of the average and median results for individual stations. While a number of methods for determining durations are available, our preferred solution is the median of the high-frequency results, as the high-frequency outputs most consistently report clearer information, and medians do not suffer from long-tailed outliers. Thus, new high-frequency median TACER duration for an event is hereafter called T_{TACER}.

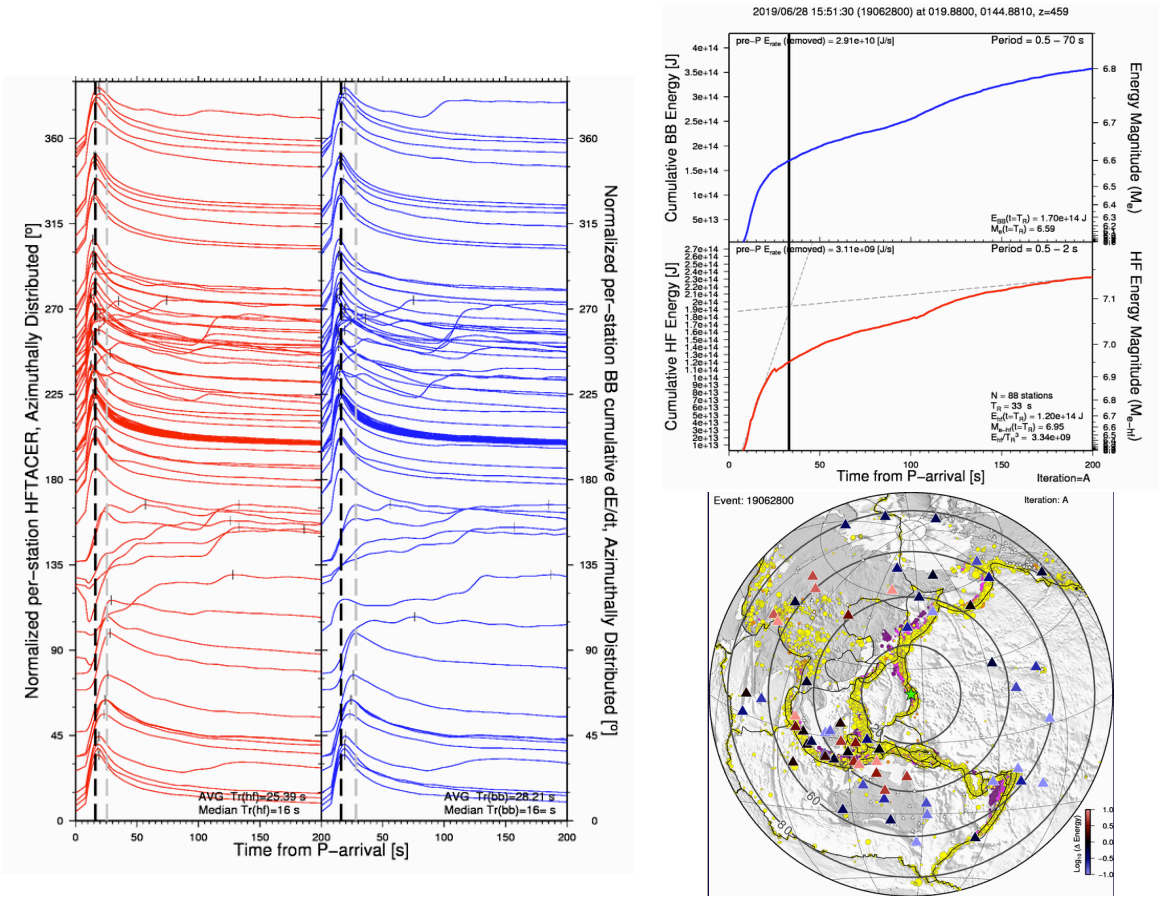

Figure 1: Real-time results for *RTerg* showing updated code output for an individual earthquake (2019/06/26, evid=19062600) as a result of this project. [Left] The azimuthal distribution of TACER results are shown, identifying the approximate rate of peak energy growth over time from the theoretical P-arrival. The algorithm determined peak is shown as a small vertical bar on each colored curve, with the average and median (preferred) times from the entire dataset reported at the bottom (both 16 s in this case). Colors denote the high-frequency (0.5-2s) and broadband (0.5 and 70s) results. [Top-right] Also shown are the cross-over duration (T_{XO}) and the cumulative energy determinations at that time both in high-frequency and broadband. The broadband energy (E_{bb}), and its conversion to energy magnitude (Me), are well established (1.7e14 J, M_e=6.59). [Bottom-right] A hemispheric map view highlights the event location and station distribution, reporting the spatial variability in energy results.

Performance:

We initially evaluate the performance of the new determinations of rupture duration from TACER (T_{TACER}) relative to the older cross-over duration (T_{XO}) determined from the stacked energy growth at high frequency (shown in top of Figure 1). For comparisons, we look at our real-time results obtained between 2009 and early 2020, for events with initial reported magnitudes greater than 6.5. We also only evaluate events in which at least 20 stations reported with clean and clear data (as determined by algorithm). Our resultant dataset contains 657 events and 46,388 waveforms from global events. We report find that T_{TACER} regularly reported shorter durations than did T_{XO}, as is expected given that the later stacks all energy growth curves for a unified result that will bias toward a result in stations where energy is dominant later (e.g. away direction of a unilateral rupture, or stations where signals are dominated by modestly delayed depth phases). Across all events, we found that there was an approximately 31% reduction in duration from the original T_{XO}.

This difference is greater for earthquakes deeper than 70 km (40%), where T_{TACER} better isolates the initial depth-phase (Figure 2). This increase in reduction is about constant for all deeper events.

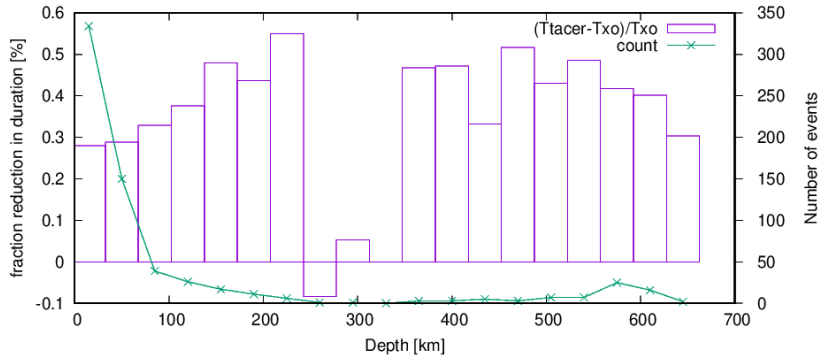

Figure 2: Reduction in duration as an function of depth for event durations determined using T_{TACER} as compared to T_{XO}. Results are binned in 30km depth sections (magenta boxes), and are reported with the number of earthquakes recorded in each (green lines and points). The average for the entire dataset is 30%, reflecting increased variance in deeper events.

The results are also shown as a function of energy (Figure 3). Here, the difference between durations are quite apparent, as T_{TACER} very consistently is shorter than T_{XO} for most events, and a clear even earlier trend is seen for events deeper than 70 km depth, due to separation of depth phases. Here, one can also begin to explore the variability in results from individual stations around the median duration. Because of long-tails that tend to make individual event results appear as a truncated log-normal rather than a more simple Gaussian distribution, we chose to report the points that contain the bottom and top 75% of data, rather than standard deviations. This too is more appropriate given our preferred solution is a median rather than a mean.

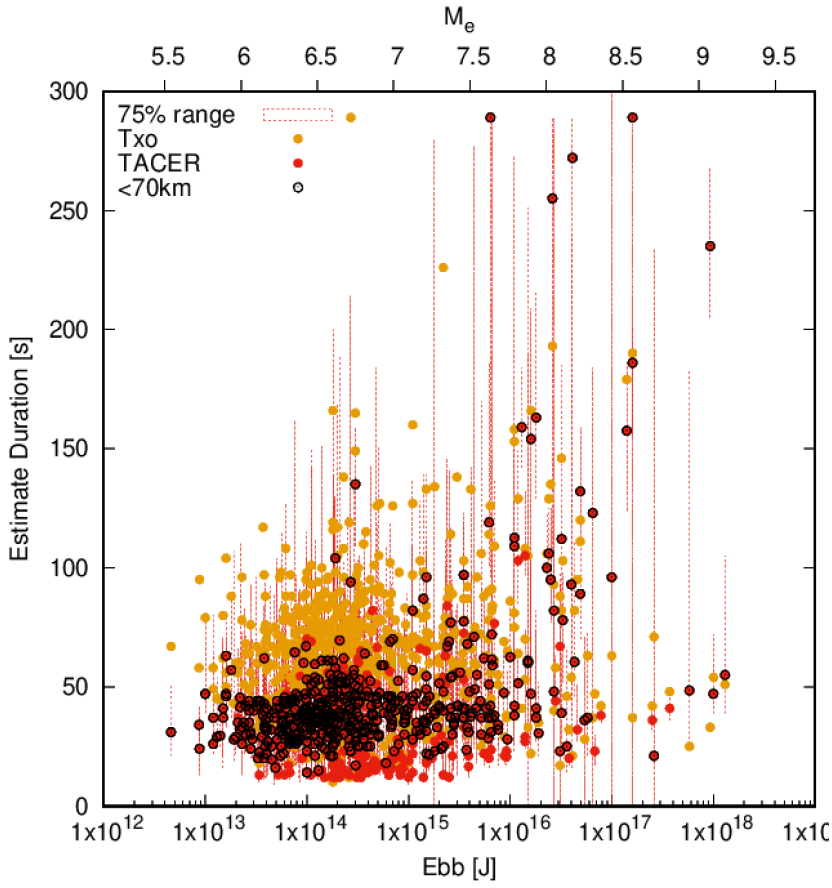

Figure 3. Broadband energy (Ebb) is shown with two methods for determining and reporting earthquake rupture durations. The durations are from either the older cross-over duration (T_{xo}; yellow circles) method, or from the newer TACER method (T_{TACER}; red circles), and are shown for events with initial magnitudes greater than 6.5, and more than 20 stations reporting. First, the composite cumulative energy (Ebb) for an event (x-axis) is determined as a singular value at the median of the composite TACER. TACER durations for events shallower than 70 km depth are circled. These events tend to report later than many deeper events which identify the direct and depth phases separately. Also noted, newer T_{TACER} durations, while giving information on variability, also yield are generally shorter than the prior T_{xo} duration that required all data to be initially stacked.

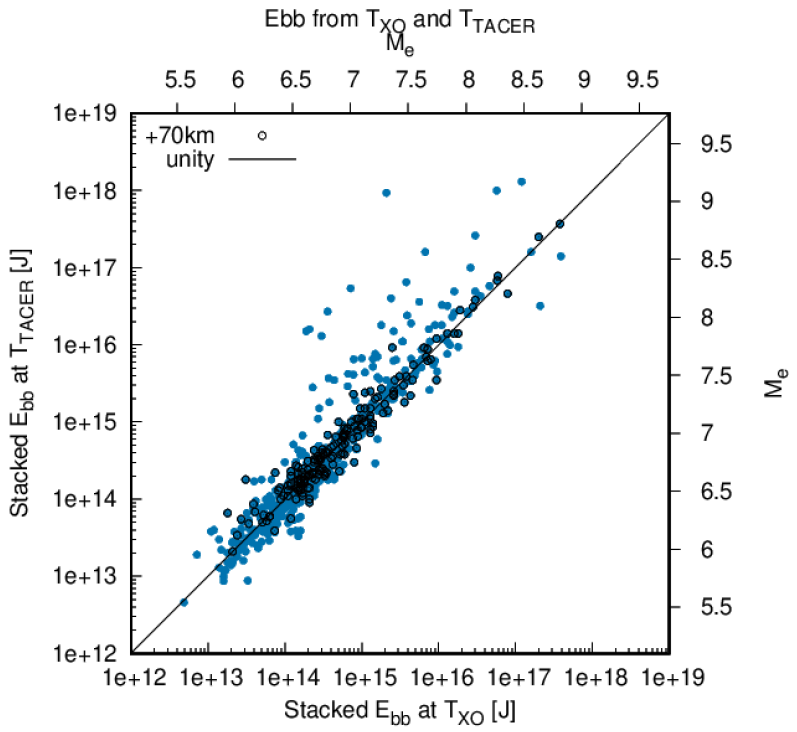

Figure 4. Broadband energy (E_{bb}) are shown as determined from two methods for events shown in prior figures. First, E_{bb} is reported at T_{xo} form the composite cumulative energy for an event (x-axis). New here, we also report E_{bb} as a singular determined value at T_{TACER} (y-axis). Data are also differentiated for events deeper than 70km, which generally show less variability in method. Results show that the methods largely agree, however there are notable outliers that need to be further explored.

Finally, because a new determination for duration is being routinely made we also evaluate the functionality of using it for the cut-off in our determinations in energy rather than using the original cross-over method. Figure 4 shows the range of energy results calculated using T_{XO} vs T_{TACER}. Results are quite comparable, though some notable outliers exist that need to be further explored. Secondly, we can explore using individual station results for energy as well, by using the per-station calculation of T_{XO} and calculate the broad-band energy growth at that station at that time. Results for a comparison of energy as calculated by these two methods show again that they're comparable (Figure 5), but again there are some modest differences. Overall, for smaller magnitude events (below about Me 7.4) results are nearly the same, but larger events appear modestly smaller, when using the range of Ebb solutions obtained across the network.

An algorithmic advantage of this method, beyond being determined per-station, is that the method can reduce the delay before final determinations are made as only one solution needs be made per station after enough data is collected to obtain a maximum in the TACER. Having that result, the algorithm only needs to run on additional stations as they too obtain sufficient data for a TACER solution, giving updates to preliminary estimates based on less information. Currently, the algorithm reprocesses each station and merges results for a singular cumulative energy growth since individual energy growth results were found to be quite erratic, and functioned poorly in unsupervised algorithms.

Figure 5. Broadband energy (E_{bb}) is determined from two methods for events shown in prior figures. First, the composite cumulative energy for an event (x-axis) is determined as a singular value at T_{TACER}. E_{bb} is also calculated from the per-station cumulative energy (y-axis) for the TACER time determined for that individual site. Data are also differentiated for events deeper than 70km. This second method, giving individualized solutions per waveform, yields uncertainty information about an event's solution space, and can be programmed to give results more rapidly, as per-stations solutions are possible. Solutions are quite similar for smaller events (below ~Me7.4), but start to diverge modestly for some of the larger events.

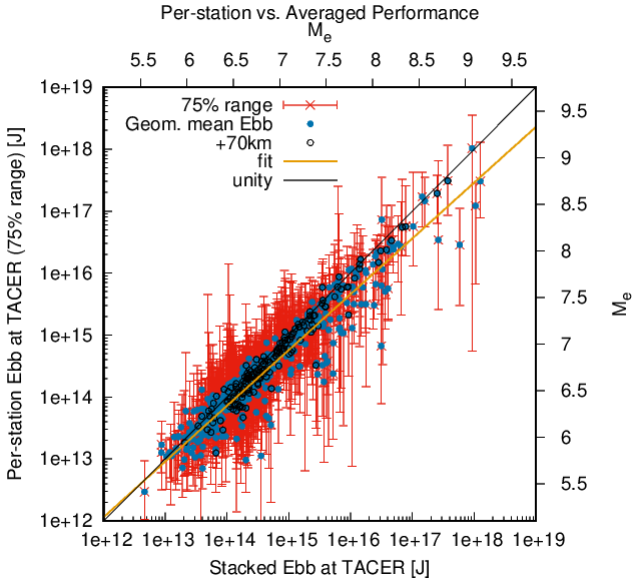

Deep earthquake identification and characterization:

Because we found that deep earthquakes pose a problem with multiple peaks, we determined it was necessary to explore the development of a method to differentiate and automatically determine multiple peaks associated with the separation from *P*-phase and the first depth phase (*pP)* at teleseismic distances (Figure 6). An algorithm that automatically identifies these events too, would be useful for quick-checking the rapid location information that we use to initiate our runs, as a poor depth can severely limit performance, and create a bias in event duration and energy estimates. This algorithm development and study too was used to train graduate student, Louisa Barama, in my lab.

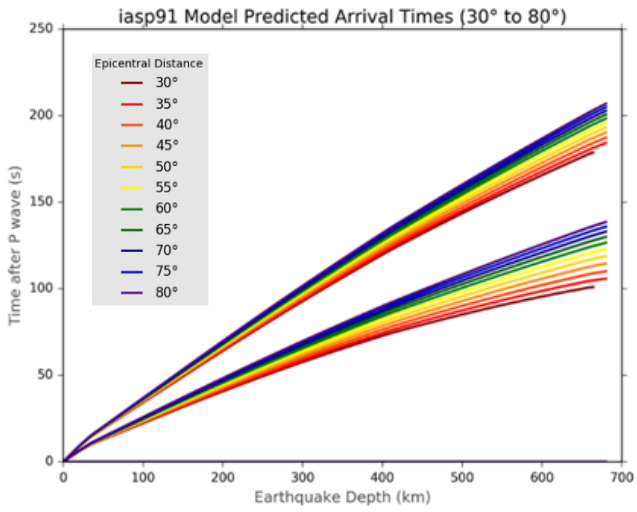

Figure 6. Theoretical arrival times for depth phases, *pP*- and s*P*-, relative to the direct *P*-phase (0 time) as a function of event depth (x-axis), and station distance (color), determined using the IASPEI91 earth model, as predicted from the algorithm *TauP*.

1.Deep Earthquake Rupture Duration

Initially, we investigated the relationship between scaled rupture duration and earthquake depth. Following the method of Houston (2001) we used earthquake rupture determinations from *RTerg*

for gCMT events globally with moment magnitude greater than 6.5 that occurred from 2014 to 2017. We chose these events and catalog to start because of a requirement for improved location and depths over our initial catalog. To remove the effect of seismic moment and to allow direct comparison and averaging of different magnitude events, these rupture durations were scaled by the cubed root of the moment, using the equation for scaled duration (t), below.

$$t = \left[\frac{M_{0ref}}{M_0^i}\right]^{\frac{1}{3}} \tau$$

Where, M_{0ref} = 10^{19} Nm, τ is the unscaled rupture duration time, and M_0^i is event global centroid moment-tensor (CMT) moment. For better accuracy compared to the initial National Earthquake Information Center (NIEC) reported earthquake nucleation depths, CMT depths were also used for each earthquake in this study. Our results (figure 7) correspond to the findings from Houston (2001) that with increasing depth there is a decrease in scaled rupture duration time, with a significant shortening of rupture duration at ~ 100 km depth and a drop off of the quantity of events beyond ~ 40km depth.

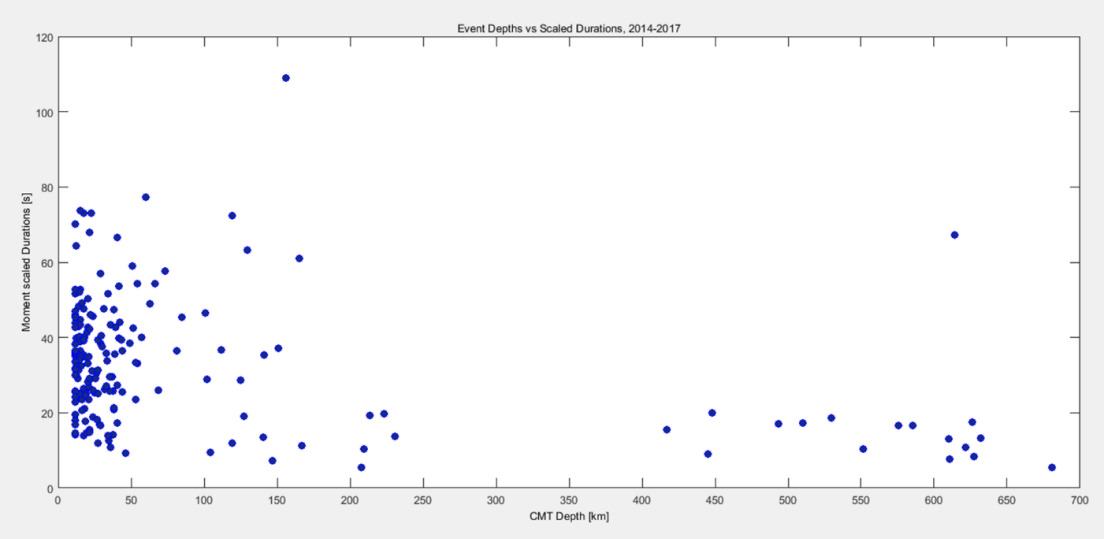

Figure 7. Earthquake depth (reported by gCMT) compared to scaled rupture duration following the method of Houston (2001).

Deep Earthquake Radiated Energy

This study explored the use of earthquake radiated energy determinations by Convers and Newman (2011 and 2013) to discriminate depth phases from initial pulses of earthquake energy without any additional processing of the waveforms. We then explored applications for these observations of the energy peak characteristics of deep earthquakes. One problem we sought to address is the complications for radiated energy and rupture duration determinations for deep earthquakes. The existing *RTerg* algorithm attenuation correction for real-time calculations of earthquake radiated energy and duration are for shallow earthquakes where the direct (*P*) and depth phases (*pP* and *sP*) all travel along similar paths. For deeper earthquakes, the depth phases become distinctly separated from the direct arrival and thus the attenuation of the short upgoing ray of the depth phases cannot be ignored (Okal, 1992). Since depth phases arrive later than the direct *P* for deep earthquakes, the rupture duration reported can be substantially artificially lengthened.

To implement the results of this work for detection of deep earthquakes in real time, all measures and actions taken on the data were ones that can be applied with no *a priori* knowledge about the event. We used global earthquakes with moment magnitude greater than 6.5 from 2008 to February 2019. Since the real-time depth calculations are not reliable, Engdahl Catalogue event depths for events through 2015 and Advanced National Seismic System (ANSS) depths are used for events occurring after where Engdahl depths are not available. We evaluate the per-station energy flux obtained from P-wave group energy calculations by Convers and Newman (2011 and 2013). The first-derivative of the per-station energy growth time series for each event is used to identify peaks of energy associated with the direct-*P* and depth phases (*sP, pP*), see Figure 8.

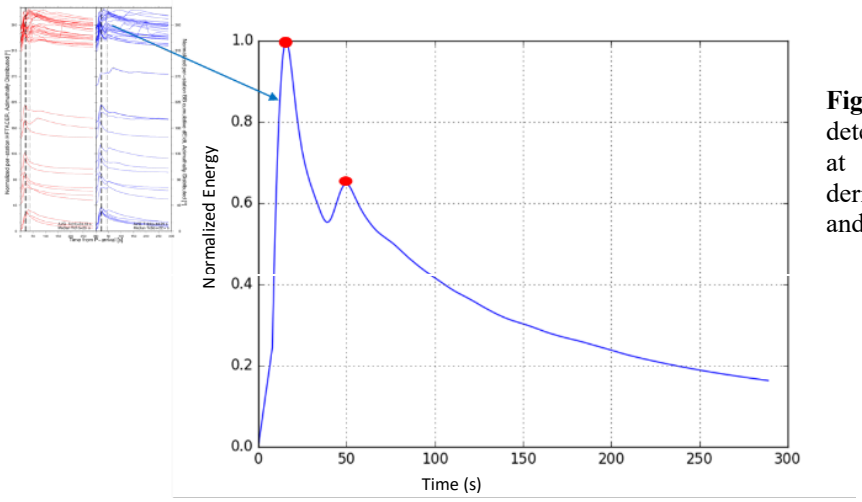

Figure 8. Single station peak determination for an event reported at 124 km depth. The first derivatives, show as peaks in energy, and are identified with red dots.

As observed in figure 9, for depths ≥ 70 km, we observed a clear separation of the energy peaks, *P* and combined *pP* and *sP* energy, as we expected (and hoped). When compared to the predicted arrival times, our results appear to be offset in time, especially at deeper depths, possibly due to an increase contribution of other phases at these later times. Other smaller variations in the arrival times for phases are likely due to heterogeneities in mantle velocity structure, errors in location, and changes in the faulting process (from frictional to possibly transformational faulting) with depth (Vidale & Houston, 1993).

The times of the largest number of energy peaks per station per event, are compared to predicted arrival times calculated using the iasp91 velocity model (Kennett and Engdahl, 1991) for the *pP* and *sP* depth phases for stations 30 to 80 distance degrees from the source at depths 0 to 700 km.

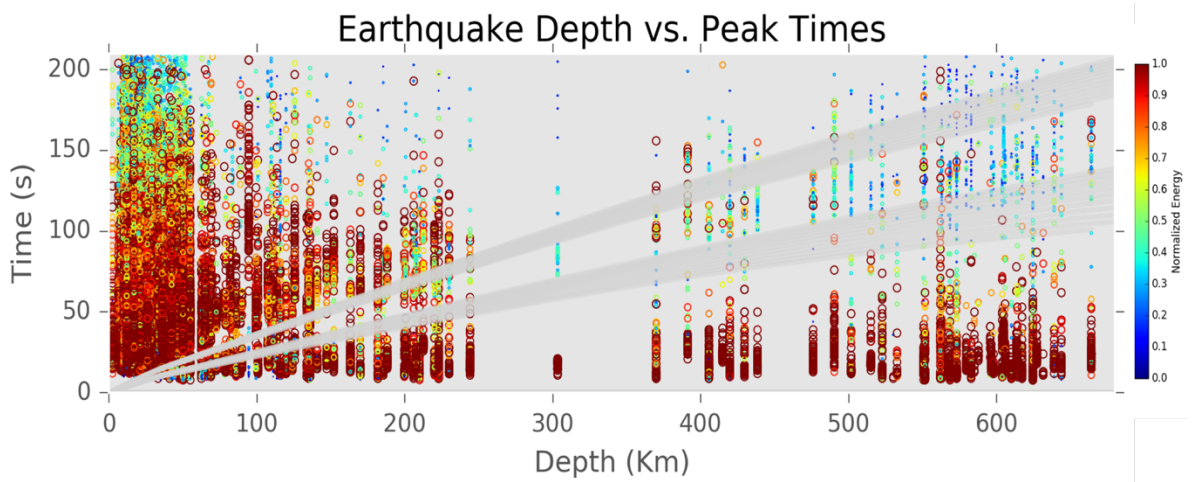

Figure 9. First and Second temporal energy peaks for all stations for each event plotted with the predicted *pP* and *sP* arrival times calculated from the iasp91 velocity model. Color and size of data circles represent the corresponding normalized energy (0 -1) value for time of peak in the energy flux time series.

To discriminate deep earthquakes from shallow earthquakes, we compare results of the broadband to high-frequency data sets. What we observe is that (as theory would predict) the energy pulses from the depth phases *pP* and *sP* become sufficiently attenuated due to their longer ray paths and triple interaction with the crust and upper lithosphere. This gives us a reliable double-hump discriminant for deep earthquakes that is applicable in real-time. For these events, we intend to only retain the direct *P*-wave information for duration and energy calculations, not possible for shallower events. Such a treatment, while seemingly easier will limit real-time single-station viability and require more averaging, as a lack of information of the focal sphere will yield more per-station variability. Figure 10 shows the high-frequency and broadband calculation comparisons for earthquakes of depths of 12.2 and 209.9 km with energy magnitudes of Me 6.11 and 6.81 respectively.

Thus far in this study, we have successfully identified reliable energy characteristics that are diagnostic of deep earthquakes. These characteristics will be useful for both identifying these events, and for creating independent parameters for real-time energy and duration calculations, particularly at teleseismic distances. The motivation for continuing this work is rapid and robust identification of deep earthquakes and the application of more accurate real-time analysis. Currently, we are building algorithms that discriminate between shallow (less than 30 km) and deep earthquakes (greater than 70 km) using the difference in energy peak results in broadband and high frequency bands, for the implementation of real-time. A portion of this study was presented at the 2018 American Geophysical Union Fall meeting, abstract and poster identification number S33E-0637.

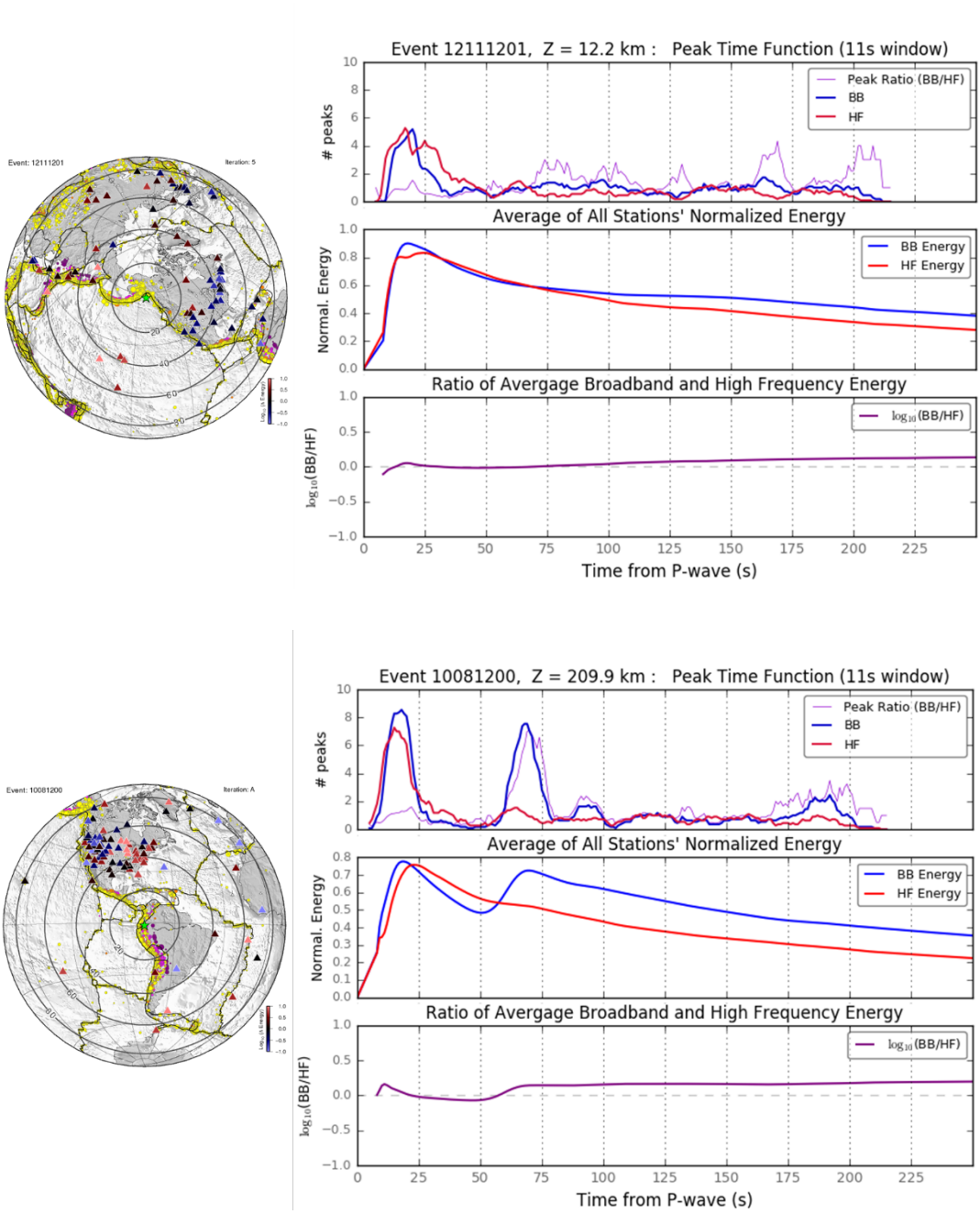

Figure 10. (top plot) Event 12111201 and (bottom plot) Event 10081200. The top graph for each event plot shows the number of peaks of energy that occur in 11 second time windows for all stations for each event. The middle plot shows the real-time normalized energy (from Georgia Tech real-time energy determinations) averaged for all stations for each event and the bottom plot shows the ratio of broadband and high frequency energy of the normalized energy plot above it.

A surprising secondary result of this study was that we reliably identified extended rupture durations in the depth window around each the 410, 520 and 660 km discontinuities. (See figure 11). This is very similar to the result of Vidale & Houston (1993), that found earthquakes in the α-olivine stability field region display the large variations in rupture duration (above 410 km), with moderate variation in the β-phase (above 520 km), and the least variation in the γ-phase (above 660 km). Houston (2001) also found earthquake durations to be generally consistent between 350-550 km with an abrupt decrease in duration below 550 km depth.

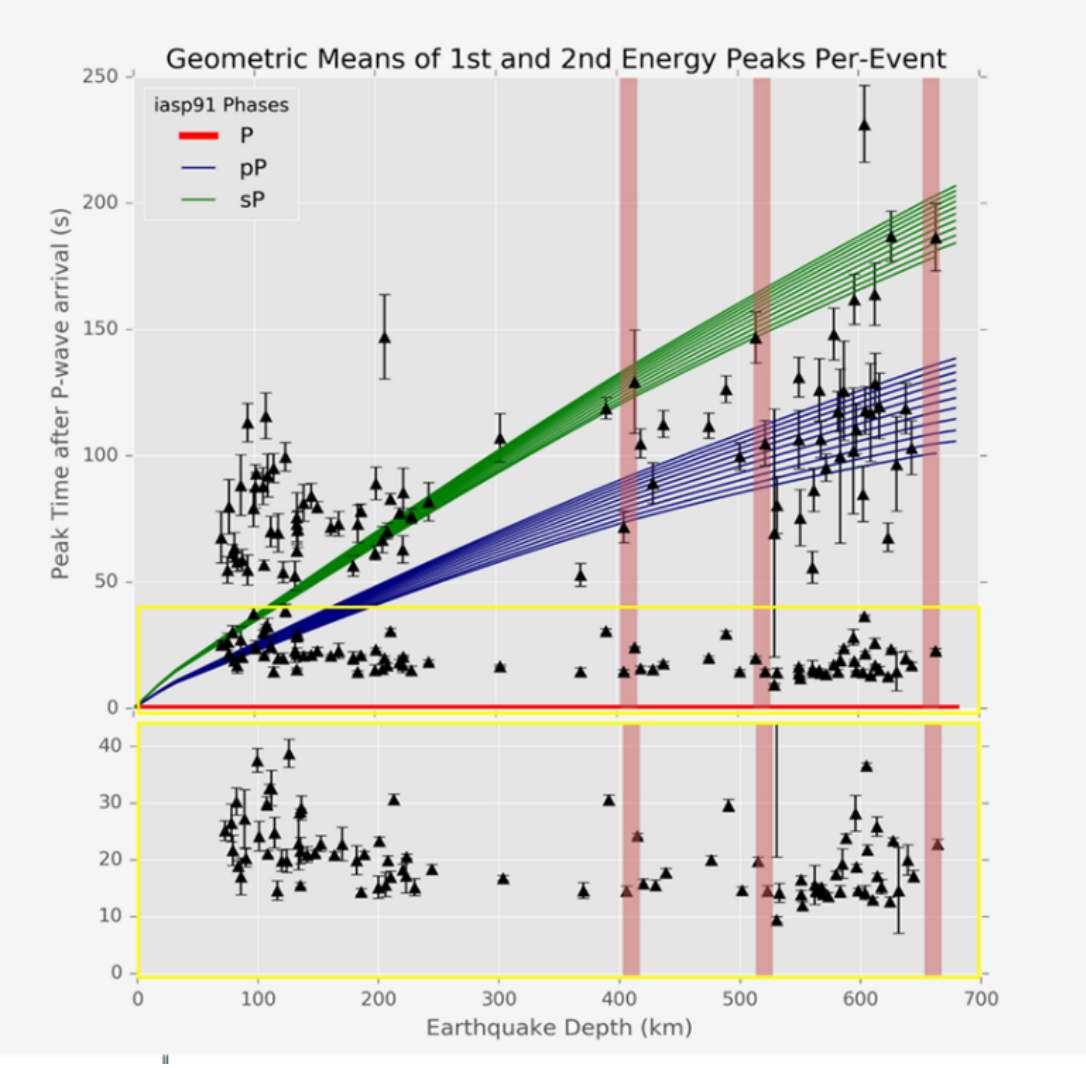

Figure 11: Geometric average (black triangles) of the first and second temporal peaks for every station for each earthquake in the dataset. Red, blue and green lines represent the phases P, pP, and sP predicted arrival times. Red bars represent the 410, 520, and 660 km discontinuities (Faccenda and Zilio, 2017).

Near-field Energy:
As a follow-on to some of this work, and in exploring the full-python development of this code, L. Barama has most recently begun developing versions of these algorithms to work in the near-field. This work is ongoing, but would be extremely useful for very rapid determination of source parameters for earthquake and tsunami early warning. Should single-station results in the near-field prove reasonable, these methods may too work for single-station results performed with only a local sensor and processor, without need for internet communication.

Products:
We are working on papers to write-up the depth-dependence component of the algorithm, and have reported on this research at the 2019 Fall AGU (Barama et al., 2019). Too, the initial development from this work was reported in context of its testing in a regional environment surrounding the Solomon Islands in Fall 2016 (Barama et al., 2016). Because of problems with development of full python-version of code, we did not implement algorithms directly at the NEIC as of yet.

Bibliography: Outcomes from this project denoted with a leading *

*Barama, L., A. V. Newman, J. A. Convers, A Search for Characteristic Seismic Energy Radiation Patterns to Identify Possible Fast-Rupturing Activity Associated with Tsunamigenic and Other Earthquakes Around the Solomon Islands, Abstract presented at the Fall AGU meeting, 2016.

*Barama, L., A. V. Newman, Discriminating Depth Phases from Earthquake Energy for Automated Real-time Assessment, American Geophysical Union Fall Meeting, Washington, DC, USA, 2018. ID: S33E-0637.

Convers, J.A., and A.V. Newman (2011), Global evaluation of large earthquake energy from 1997 through mid-2010, J. Geophys. Res., 116, B08304, doi:10.1029/2010JB007928.

Convers, J.A., and A.V. Newman (2013), Rapid Earthquake Rupture Duration Estimates From Teleseismic Energy Rates, with Application to Real-Time Warning, Geophy. Res. Lett 40, 1-5, doi:10.1002/2013GL057664.

Faccenda, M. & Dal Zilio, L. The role of solid–solid phase transitions in mantle convection. Lithos 268, 198–224 (2017).

Houston, H. (2001). Influence of depth, focal mechanism, and tectonic setting on the shape and duration of earthquake source time functions. Journal of Geophysical Research, 106(B6), 11,137–11,2150. https://doi.org/10.1029/2000JB900468.

Kennett B.L.N. Engdahl E.R. , 1991. Traveltimes for global earthquake location and phase identification, Geophys. J. Int. , 135, 429–465.

Newman, A.V., and J.A. Convers (2013), Real-Time Earthquake Energy and Rupture Duration Determinations, http://geophysics.eas.gatech.edu/RTerg/, Atlanta, Georgia.

Okal, E. A., A student's guide to teleseismic body wave amplitudes, Seismol. Res. Lett., 63, 169–180, 1992.

Vidale, J., and H . Houston (1993), The depth dependence of earthquake duration and implications for rupture mechanisms , Nature, 365,45–47, doi:10.1038/365045a0.